



Design and optimization of a soft X-ray tomography system on Keda Torus eXperiment



Yiming Zu^a, Wenzhe Mao^{a,*}, Tao Lan^a, Weixing Ding^{a,c}, Ge Zhuang^a, Sen Zhang^a, Hangqi Xu^a, Junfeng Zhu^a, Jinlin Xie^a, Hong Li^a, Adi Liu^a, Shoubiao Zhang^b, Chu Zhou^a, Zixi Liu^a, Zian Wei^a, Zhengwei Wu^a, Chijin Xiao^{a,b,d}, Wandong Liu^a

^a University of Science and Technology of China, Hefei, Anhui 230026, China

^b Institute of Plasma Physics, Chinese Academy of Sciences, Hefei 230031, China

^c University of California Los Angeles, Los Angeles, CA 90095, USA

^d Plasma Physics Laboratory, University of Saskatchewan, Saskatoon, SK S7N 5E2, Canada

ARTICLE INFO

Keywords:

Quasi-single-helicity
Soft X-ray
Bayesian experimental design
Tomographic reconstructions

ABSTRACT

We report about the soft X-ray (SXR) tomography system which is being developed on Keda Torus eXperiment (KTX). The tomographic system aims at studying three dimensional effects in reversed field pinch with high plasma current, particularly in quasi-single-helicity state (QSH). The view distribution of the probes has been carefully designed to reflect the experimental constraints. Bayesian experimental design (BED) is used to optimize the signal camera location and camera opening angle, aiming at maximizing the gain information in future QSH states. The BED approach allows us to quantitatively evaluate the performance of the design, and to estimate the design robustness. The physical image of the plasma is tomographically reconstructed using Cormack approach and the reconstructed emissivity image may be compared to the emissivity model using the residual error χ . The camera location, camera opening angle, and sightline density are finally decided by quantitatively comparing diverse designs in order to achieve the best reconstruction.

1. Introduction

Tomography is an extremely powerful technique in advanced fusion devices like ITER [1] and the soft X-ray (SXR) tomography systems had been already installed in some high power plasma experiments like JET [2], DIII-D [3] and RFX-mod [4]. One of the main reasons for its success in plasma physics is its non-invasive character, which allows one to image the plasma radiation emissivity distribution [4]. The emissivity is then used to study several plasma properties, such as the shape of the configuration, the magnetohydrodynamics (MHD) phenomenology and the particle and energy transport. The magnetic confinement fusion device is a complex system, and the diagnostic design should consider both scientific objectives and technological requirements. It is thus crucial to develop a universal quantifiable approach for diagnostic design.

In this paper, we report about the design of a SXR tomography system for Keda Torus eXperiment (KTX) based on quantitative methods. The middle-sized KTX device is a reversed field pinch (RFP) machine in

China [5,6]. The research priorities of KTX include a better understanding of RFP physics and technology, with focus on the improvement and self-organization of RFP confinement, and also include technological development. A relevant issue to improve confinement in RFP is the self-organization of the RFP plasma towards the single-helicity regime, where one mode dominates the plasma dynamics, and the remaining secondary modes are reduced in amplitude [7]. This plasma state in an RFP is called quasi-single-helicity (QSH) state [8], and is likely to become one of the future research topics of KTX. It is thus essential to develop an SXR tomography system to directly image the QSH state.

Two main challenges should be considered in the SXR design: estimating the expected data from future experiments, and quantifying the benefit of a design [9]. The Bayesian approach is definitely suitable to deal with those challenges, and it has been applied to multichord interferometer design on Wendelstein 7-X [10,11]. The physical image is studied by tomographic reconstruction of SXR emissivity [12], and the design parameters may be optimized by minimizing the errors between the reconstructed results and emissivity model.

* Corresponding author.

E-mail address: maozhe@ustc.edu.cn (W. Mao).

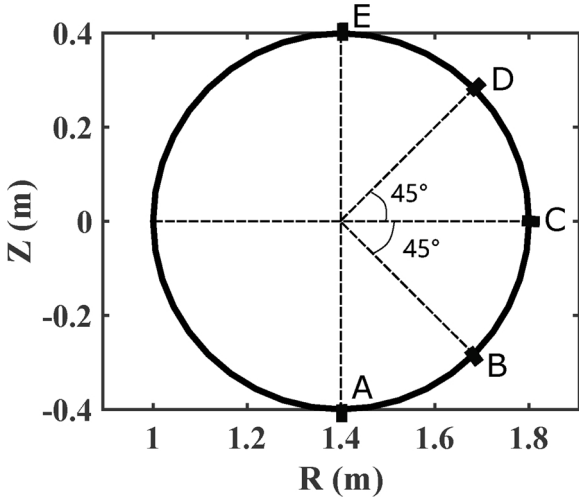


Fig. 1. The SXR windows on KTX, marked by A, B, C, D and E.

The rest of this article is organized as follows. In Section 2, the Bayesian experimental design principle, and the case study of SXR design are described. The tomographic reconstruction of SXR emissivity, which depends on Cormack approach, and in the specific design is discussed in Section 3. Section 4 gives the conclusion of this article.

2. Lines of sight design of SXR tomography using Bayesian experimental design

2.1. Bayesian experimental design

The merits of an experimental design may be evaluated by means of a utility function $U(D, \eta)$ which depends on the experimental data D , and the design parameters η . The function contains a diagnostics model (such as the 2D SXR emissivity model), and also the expected range of the parameter α of interest (such as an expected plasma axis shift range). The design parameters are understood as quantities characterizing the experimental setup and the diagnostic unit, and are assumed accessible and tunable (such as the location of SXR camera).

The evidence of the data is represented by the conditional probability density function $P(D|\eta)$, and the expected utility function (EU) can be obtained as the average over the range of expected data:

$$\text{EU}(\eta) = \int dD P(D|\eta) U(D, \eta), \quad (1)$$

which depends only on the design parameters η .

By using Kullback–Leibler distance and Bayesian theorem [11], Eq. (1) may be written as:

$$\text{EU}(\eta) = \iint dD d\alpha P(D|\alpha, \eta) P(\alpha) \log \left[\frac{P(D|\alpha, \eta)}{P(D|\eta)} \right], \quad (2)$$

where $P(D|\eta)$ can be obtained by integrating $P(\alpha)$ and $P(D|\alpha, \eta)$. In the following, we use a uniform distribution for $P(\alpha)$ in the interval $\{\alpha_{\min}, \alpha_{\max}\}$

$$P(\alpha) = \frac{1}{\alpha_{\max} - \alpha_{\min}}, \quad (3)$$

and a Gaussian likelihood

$$P(D|\alpha, \eta) = \frac{1}{\sigma\sqrt{2\pi}} \exp\left(-\frac{(D - f(\alpha))^2}{2\sigma^2}\right). \quad (4)$$

Here $f(\alpha)$ is a mathematical model of the experimental set-up describing the emergence of a data point at a certain state of α and σ is the standard

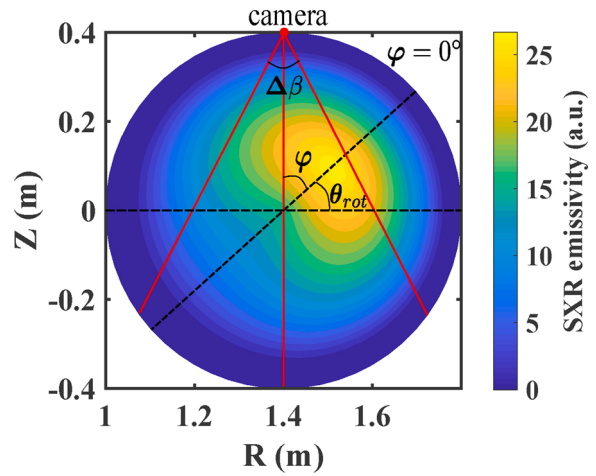


Fig. 2. Simulated SXR emissivity in QSH state and the definition of design parameters. The plasma is axisymmetric with the $\varphi = 0^\circ$ plane. φ is the angle of single camera location, θ_{rot} is the rotation angle of plasma and $\Delta\beta$ is the SXR camera opening angle.

deviation of the measurement noise. Eqs. (3) and (4) can then be used to determine the expected utility function which is shown in [10].

2.2. Case studies

The design studies are performed for a single SXR camera investigating the QSH state. The QSH states have been confirmed experimentally in several RFP device, where the innermost resonant $m = 1$ mode is dominating over the others (secondary modes) [8]. KTX is an RFP device ($R = 1.4$ m, $a = 0.4$ m) with a circular cross-section. Several constraints should be considered for SXR camera designs, such as the size and location of the available windows, the relatively high electromagnetic noise level around the machine, and the limitations of the external space. In this case, only the lines of sight have been considered, and it is assumed that the camera is located at the shell radius. The possible SXR windows for KTX at a poloidal cross-section are shown in Fig. 1. The SXR emissivity, calculated based on the assumed electron temperature T_e and density n_e [13], in a QSH state is shown in Fig. 2. Different plasma geometries and shapes are used to analyze the performance of the design algorithm.

For the creation of virtual data, the following parametrized emissivity function has been used,

$$g(\alpha_1, \alpha_2, \alpha_3) = \alpha_2 \cdot A \sqrt{[r \cos \theta - \alpha_1(1-r)]^2 + (r \sin \theta)^2} \cdot (1-r)^{\alpha_3}, \quad (5)$$

where the parameters α_1 , α_2 , α_3 represent the emissivity axis shift, maximum emissivity and edge, and A is a constant. r and θ are the plasma coordinates. The profiles of emissivity are shown in Fig. 3, assuming $\theta = 0^\circ$.

Fig. 4 gives an example of single SXR line of sight result using BED for edge estimation. The expected utility function EU reaches the maximum value when the line of sight crosses the plasma edge, which is consistent with the intuitive guess. For SXR design, the sightline of SXR should be integrated with the camera opening angle $\Delta\beta$, as in Fig. 2.

Fig. 5 shows the expected utility function, which is an integral value with the line of sight, for a single camera. The result indicates where the camera should be located to get the maximum signal-to-noise ratio (SNR). For the axis shift, the camera located at $\varphi = 90^\circ$ – 180° has maximum EU value, which indicates maximum information gain. Since the shift follows the line of $\varphi = 0^\circ$, the brightness observed by a camera with the same direction can hardly be changed. The maximum and edge have nearly the same optimum location at $\varphi = 0^\circ$. The value of edge is about 0.1 of the estimated maximum, which means that the edge has

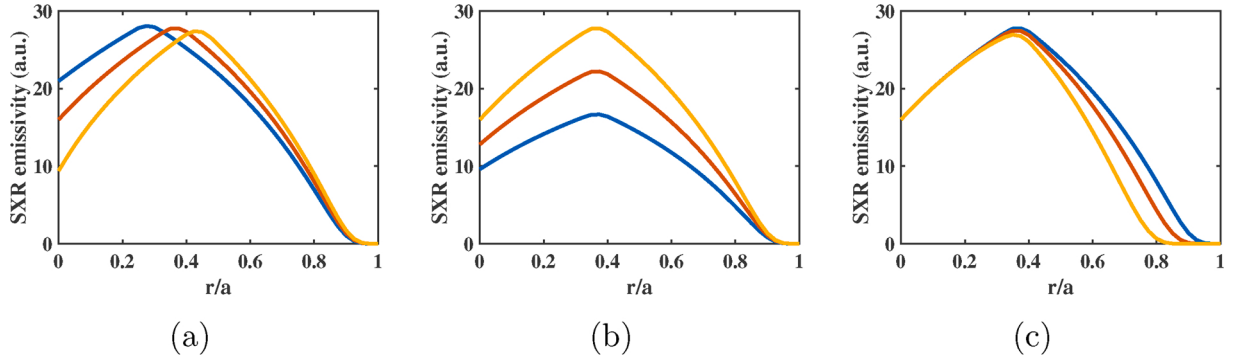


Fig. 3. The parameterized emissivity profile for estimation of the emissivity axis shift (a), maximum emissivity (b) and edge (c). The data space is generated by variation of the parameters within the following ranges: (a) $\alpha_1 = 0.4, \dots, 0.8$, (b) $\alpha_2 = 0.4, \dots, 1$, (c) $\alpha_3 = 1, \dots, 4$.

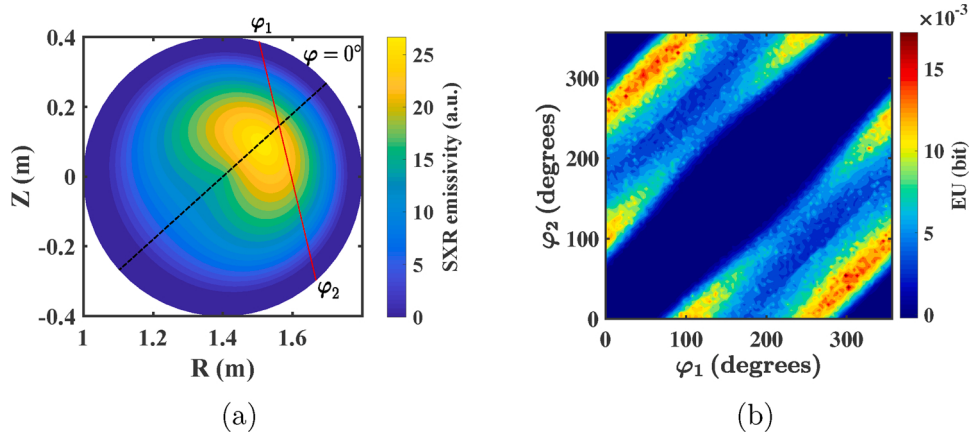


Fig. 4. Expected utility for a single SXR sightline. The angles φ_1 and φ_2 parametrize the line of sight (a), and the expected utility of sightline for edge estimation (b).

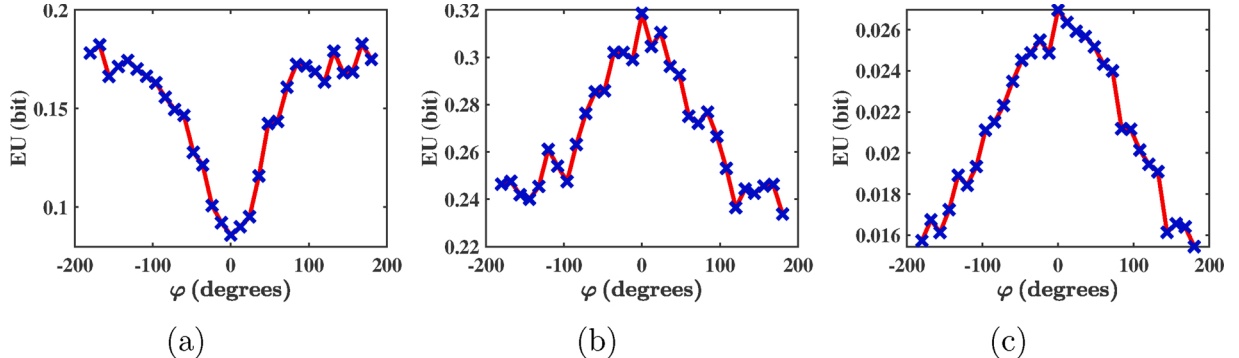


Fig. 5. Expected utility for a single camera located at φ . The three parameters are estimation of emissivity axis shift (a), maximum emissivity (b) and edge (c). EU is the integral value of the SXR chords and φ is the angle where the camera is located.

little impact on the information gain because the emissivity information is concentrated in the hot core.

Different values of statistical errors leads to different EU values. The value $\sigma = 2$ has been used in producing the above figures, and the results for $\sigma = 2, 1, 0.5$ are shown in Fig. 6. The EU value increase for decreasing σ , because EU is an expression of SNR. For the emissivity axis shift, a peak appears at $\varphi = 70^\circ$ as σ decrease, but the maximum value is still located at $\varphi = 180^\circ$. For the maximum, EU has similar shaped for $\sigma = 2, 1$, whereas it becomes more disordered for $\sigma = 0.5$. For the edge, there is always a peak at $\varphi = 0^\circ$.

Figs. 5 and 6 indicate that cameras located at $\varphi = 0^\circ$ and $\varphi = 180^\circ$ are those gaining maximum information about the parameters of interest for different σ . Considering the limitation of the windows on KTX (Fig. 1),

the two windows A and E are chosen. Since φ is in the plasma frame, the plasma should rotate ($\theta_{rot} = -90^\circ$) to make sure that $\varphi = 0^\circ$ facing window A or E.

The camera opening angle may also be studied by Bayesian theory. Fig. 7 shows the variation of the EU values with the three parameters. EU increases with $\Delta\beta$ and then saturates when $\Delta\beta$ reach 100° . As T_e is smaller near the boundary, the sightlines with $\Delta\beta > 100^\circ$ get less information than the sightlines crossing the core. This means that a camera opening angle set at 100° ensures that the SXR gain enough information.

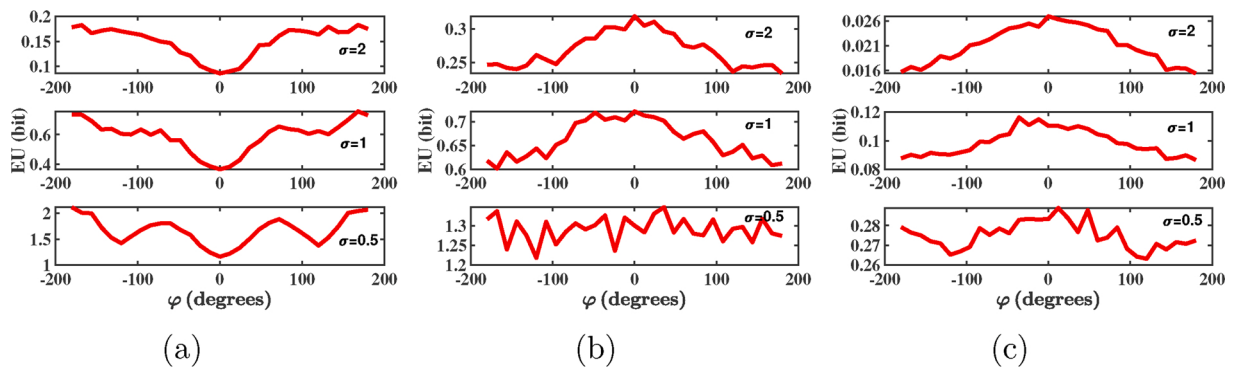


Fig. 6. Expected utility for different σ values for estimation of emissivity axis shift (a), maximum emissivity (b) and edge (c).

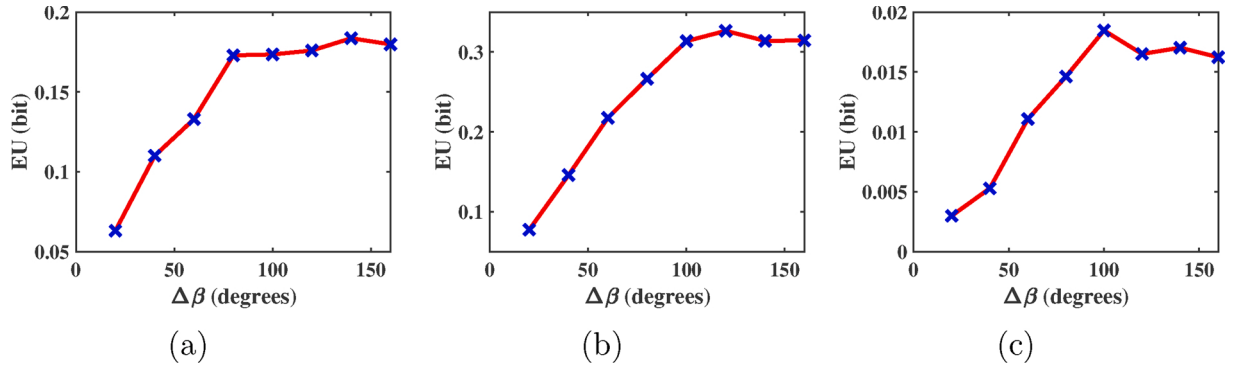


Fig. 7. Expected utility as function of the camera opening angle $\Delta\beta$. The three parameters are the estimation of emissivity axis shift (a), maximum emissivity (b) and edge (c).

3. Error analysis of SXR emissivity tomographic reconstruction

3.1. Cormack Bessel Technique

In plasma diagnostics, the measurement of SXR emissivity is carried out outside the plasma, and the signals, usually referred to as brightness, are line-integrated emissivity along the line of sight. An inversion technique is required to reconstruct the emissivity distribution image from the SXR signals [14]. Tomography is the key technique for the reconstruction of the SXR emissivity [12,15]. This is based on simultaneous multiple measurements of the SXR brightness $f(p, \phi)$ along different lines of sight $L(p, \phi)$:

$$f(p, \phi) = \int_{L(p, \phi)} g(r, \theta) d\ell, \quad (6)$$

where p is the perpendicular distance from the line of sight to the center of the poloidal cross section; ϕ is the angle that the normal to the line of sight forms with the equatorial plane and $g(r, \theta)$ is the emissivity.

The Cormack approach solves Eq. (6) by using a Bessel–Fourier series expansion of the SXR brightness and emissivity functions [16]. This is suitable for QSH states with helical structures since the measured emissivity functions are usually more localized in Fourier space than in physical space, and this makes the Cormack technique preferable to others.

In the Cormack approach, the brightness and the emissivity are expanded in Fourier series:

$$f(p, \phi) = \sum_{m=0}^M [f_m^c(p) \cos(m\phi) + f_m^s(p) \sin(m\phi)], \quad (7)$$

$$g(r, \theta) = \sum_m^M [g_m^c(r) \cos(m\theta) + g_m^s(r) \sin(m\theta)]. \quad (8)$$

The truncation is based on the number of available sightlines. Cormack proved that Fourier components of Eqs. (7) and (8) are linked by the following relations

$$g_m^{c,s}(r) = -\frac{1}{\pi} \frac{d}{dr} \int_r^1 \frac{f_m^{c,s}(\rho) T_m(p/r) p}{p \sqrt{p^2 - r^2}} d\rho, \quad (9)$$

where $T_m(p/r)$ are Tchebychev polynomials. By expanding the Fourier components over a truncated set of Bessel functions, the boundary condition of zero emissivity at the edge is met:

$$g_m^l(r) = J_m(\lambda_m^{l-1} r), \quad (10)$$

where $\lambda_m^{l-1} r$ is the l th zero of the m th order Bessel function $J_m(z)$. Then the integral relation Eq. (9) becomes a matrix equation:

$$f = W \cdot g. \quad (11)$$

The matrix \mathbf{W} defines the geometry of the system, and the emissivity vector \mathbf{g} may be found by measuring the brightness \mathbf{f} .

3.2. Error analysis and design study

In this particular design, the SXR camera aims at studying QSH state as illustrated in Fig. 2. The poloidal mode of QSH state is $m = 1$, so at least two cameras are needed for the reconstruction. Different angles between the two cameras ($\Delta\varphi$) provide different information about the parameters p and ϕ in Eq. (6). On RFX-mod and MST, the angle has been set to 90° [4,17], but there are more choices for camera location on KTX. So it is necessary to perform a quantitative analysis of the double camera locations in order to optimize the reconstruction.

The residual error χ is used to measure the reconstruction result against the SXR emissivity model.

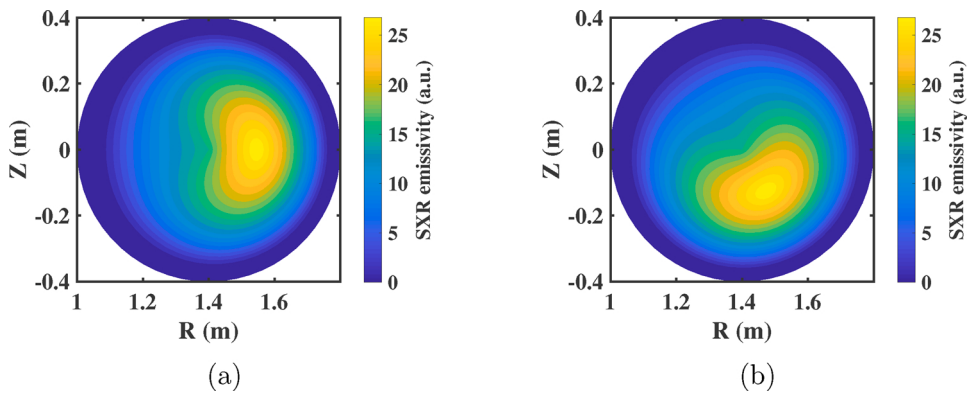


Fig. 8. The SXR emissivity model with $\theta_{rot} = 0^\circ$ (a) and $\theta_{rot} = -60^\circ$ (b).

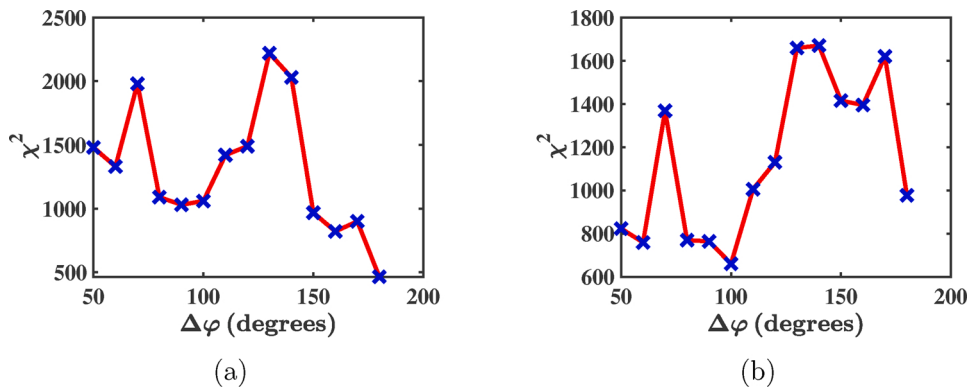


Fig. 9. The residual error between emissivity model and reconstructed result for $\theta_{rot} = 0^\circ$ case (a) and $\theta_{rot} = -60^\circ$ case (b). $\Delta\varphi$ is the angle between two cameras.

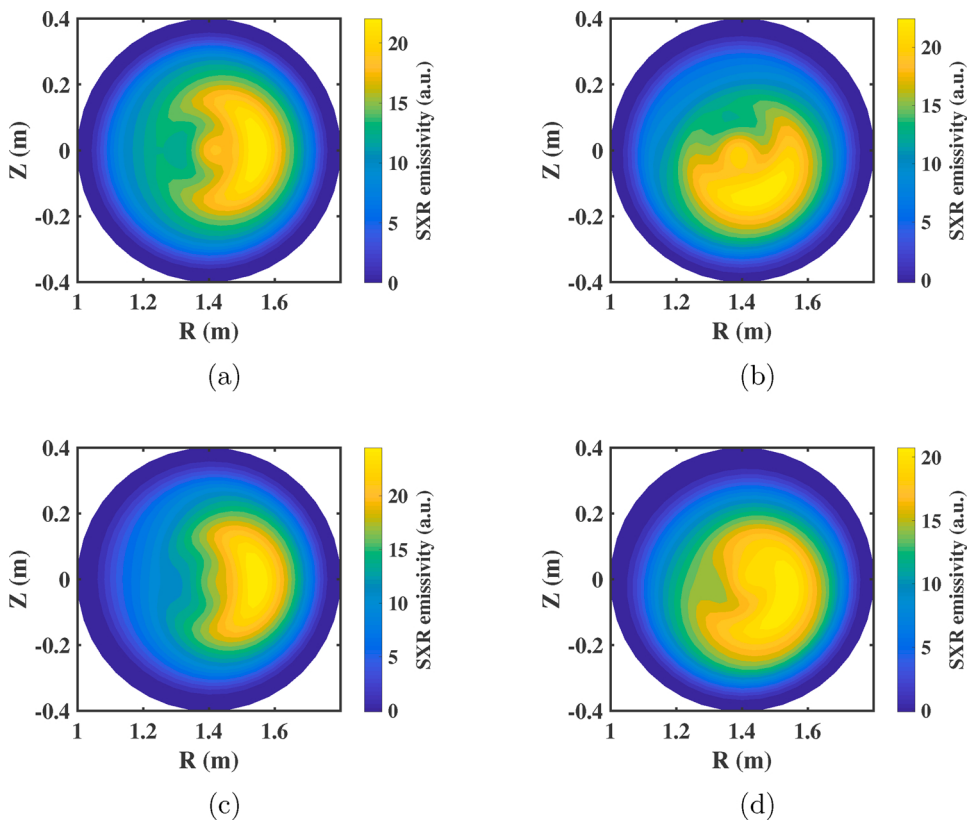


Fig. 10. Tomographic reconstruction of the SXR emissivity at $\Delta\varphi = 90^\circ$ with $\theta_{rot} = 0^\circ$ (a) and $\theta_{rot} = -60^\circ$ (b). And $\Delta\varphi = 180^\circ$ with $\theta_{rot} = 0^\circ$ (c) and $\theta_{rot} = -60^\circ$ (d).

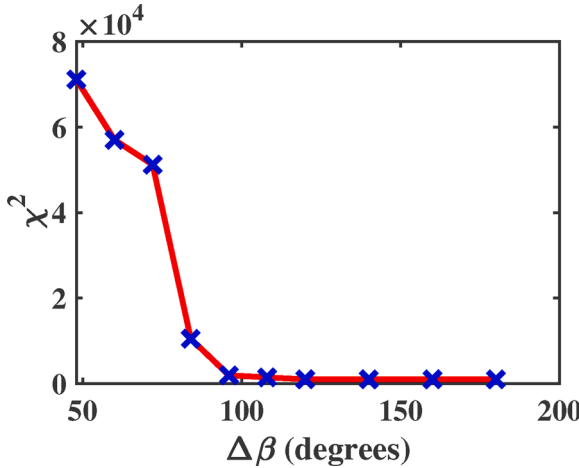


Fig. 11. The fitting result of camera opening angle.

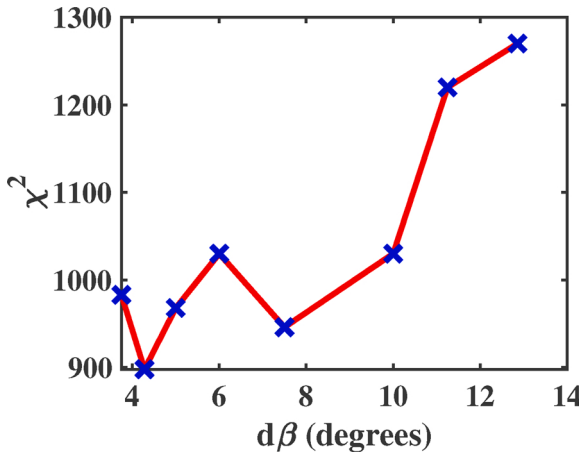


Fig. 12. The fitting result of the sightline density. $d\beta$ is the angle between neighboring sightline.

$$\chi^2 = \sum_i \frac{(D_i - M_i)^2}{\sigma^2}, \quad (12)$$

where D is the reconstructed data, M is the model and σ is the standard deviation of the measurement noise. A smaller χ^2 value indicates a better fit. Here set the two cameras to be axisymmetric with the $Z=0$ plane and two geometries of plasma have been considered. One is $\theta_{rot} = 0^\circ$ and another is $\theta_{rot} \neq 0^\circ$. θ_{rot} is defined in Fig. 2 and the models are shown in Fig. 8.

Fig. 9 shows the value of χ^2 from $\Delta\varphi = 50^\circ$ to $\Delta\varphi = 180^\circ$ with $\theta_{rot} = 0^\circ$ and $\theta_{rot} = -60^\circ$. There are two minima at $\Delta\varphi = 90^\circ$ and $\Delta\varphi = 180^\circ$ for the case with $\theta_{rot} = 0^\circ$. The contour plot is shown in Fig. 10. The reconstruction at $\Delta\varphi = 180^\circ$ is clearly better than for $\Delta\varphi = 90^\circ$. The residual error χ^2 for the $\theta_{rot} = -60^\circ$ case also gives two minima at the same angle, but the reconstruction at $\Delta\varphi = 180^\circ$ performing worse. Several $\theta_{rot} \neq 0^\circ$ cases have been computed and the results at $\Delta\varphi = 90^\circ$ are more stable when the plasma rotates. So it is more appropriate to choose $\Delta\varphi = 90^\circ$ as the angle separation between the two cameras. Since two windows has been chosen in BED, an additional window C is needed to make $\Delta\varphi = 90^\circ$ as in Fig. 1.

It is worth noting that the $\theta_{rot} \neq 0^\circ$ only shows one particular angular orientation of the plasma with respect to the two cameras, but the results are similar for other $\theta_{rot} \neq 0^\circ$ orientations. The reconstruction for $\Delta\varphi = 90^\circ$ reveals an additional hot spot (Fig. 10(a) and (b)), inconsistent with the model. This is likely due to data interpolation for p and ϕ .

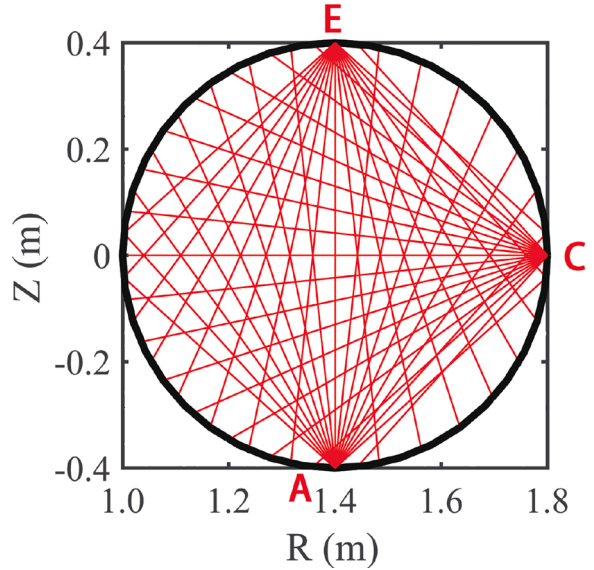


Fig. 13. The experimental design for SXR tomography cameras.

because only two cameras are used here and they give local (p, ϕ) .

The study of camera opening angle is shown in Fig. 11. It gives the same result of BED (Fig. 7), i.e. it shows that the sightlines with $\Delta\beta > 100^\circ$ can hardly gain emissivity information. As a matter of fact, the camera opening angle is usually 90° at most, because of the experimental constraints. Even if $\Delta\beta = 90^\circ$ is not the optimal configuration, it is close to the value of $\Delta\beta = 100^\circ$ and is acceptable in design.

The sightline density is described by the angle between neighboring sightlines in Fig. 12. χ^2 does not fluctuate too much when $d\beta < 10^\circ$, which indicates that the increasing sightline density makes less significant contributions to reconstructions as $d\beta < 10^\circ$. Once the camera opening angle and sightline density are confirmed, the number of sightlines of SXR can be determined accordingly. In this study, $d\beta = 6^\circ$ has been chosen for the simulation, and the number of sightlines chosen is 17, since the camera opening angle is $\Delta\beta = 96^\circ$.

4. Conclusion

SXR tomography is an important diagnostic tool for future studies of the QSH state on KTX. The goal of SXR design is to use as few hardware resources as possible.

The modeled Bayesian experimental design and tomographic reconstruction have been applied to the design of the SXR diagnostic system. The experimental design is shown in Fig. 13. Three windows have been chosen to set the SXR cameras. The camera open angle is 96° and there are 17 sightlines per camera.

The BED approach allows us to quantitatively evaluate the performance of the design, and to estimate the design robustness. Tomographic reconstruction gives the 2D reconstructed emissivity image, which may be compared to the emissivity model using the residual error χ^2 . The BED and tomographic reconstruction provide quantitative results for the design parameter η , and give a visual suggestions for the design. To the best of our knowledge, this is the first time that a Bayesian approach have been used to the design of a SXR camera system. We foresee its extension to advanced fusion devices such as ITER.

Authors' contribution

Wenzhe Mao: conceptualization, methodology, software, writing-reviewing and editing, validation, supervision, investigation. Yiming Zu: software, data curation, writing-original draft preparation, validation, investigation, visualization, writing-reviewing and editing. Chijin

Xiao, Tao Lan and Wandong Liu: writing-reviewing and editing.

Conflict of interest

None declared.

Acknowledgement

This work has been supported by the National Key R&D Program of China through the Grant Nos. 2017YFE0301704, 2017YFE0301701, 2017YFE0301700, and by the National Natural Science Foundation of China through the Grant Nos. 11635008, 11875255 and 11975231.

References

- [1] K. Hill, K. Young, M. Bitter, S. Von Goeler, H. Hsuan, R. Hulse, L.-P. Ku, B. Stratton, A. Krieger, D. Parsignault, et al., ITER X-ray diagnostic studies, *Rev. Sci. Instrum.* 63 (1992) 5032–5034.
- [2] R. Granetz, P. Smeulders, X-ray tomography on JET, *Nucl. Fusion* 28 (1988) 457.
- [3] J. Qian, L. Lao, Q. Ren, H. Rinderknecht, F. Volpe, C. Zhang, B. Wan, Equilibrium reconstruction of plasma profiles based on soft X-ray imaging in DIII-D, *Nucl. Fusion* 49 (2008) 025003.
- [4] P. Franz, L. Marrelli, A. Murari, G. Spizzo, P. Martin, Soft X ray tomographic imaging in the RFX reversed field pinch, *Nucl. Fusion* 41 (2001) 695.
- [5] W. Liu, W. Mao, H. Li, J. Xie, T. Lan, A. Liu, S. Wan, H. Wang, J. Zheng, X. Wen, et al., Progress of the Keda Torus eXperiment Project in China: design and mission, *Plasma Phys. Control. Fusion* 56 (2014) 094009.
- [6] W. Liu, W. Mao, T. Lan, G. Zhuang, J. Zheng, P. Yuan, H. Li, J. Xie, A. Liu, Z. Wu, et al., An overview of diagnostic upgrade and experimental progress in the KTX, *Nucl. Fusion* 59 (2019) 112013.
- [7] J. Sarff, A. Almagri, J. Anderson, M. Borchardt, D. Carmody, K. Caspary, B. Chapman, D. Den Hartog, J. Duff, S. Eilerman, et al., Overview of results from the MST reversed field pinch experiment, *Nucl. Fusion* 53 (2013) 104017.
- [8] D. Terranova, D. Bonfiglio, A. Boozer, A. Cooper, M. Gobbin, S.P. Hirshman, R. Lorenzini, L. Marrelli, E. Martines, B. Momo, et al., A 3D approach to equilibrium, stability and transport studies in RFX-mod improved regimes, *Plasma Phys. Control. Fusion* 52 (2010) 124023.
- [9] H. Dreier, A. Dinklage, R. Fischer, M. Hirsch, P. Kornejew, E. Pasch, Bayesian design of diagnostics: case studies for Wendelstein 7-X, *Fusion Sci. Technol.* 50 (2006) 262–267.
- [10] H. Dreier, A. Dinklage, R. Fischer, M. Hirsch, P. Kornejew, Bayesian design of plasma diagnostics, *Rev. Sci. Instrum.* 77 (2006) 10F323.
- [11] H. Dreier, Bayesian Experimental Design – Applications in Nuclear Fusion, Max-Planck-Institut für Plasmaphysik, 2007.
- [12] P. Franz, L. Marrelli, P. Piovesan, I. Predebon, F. Bonomo, L. Frassinetti, P. Martin, G. Spizzo, B. Chapman, D. Craig, et al., Tomographic imaging of resistive mode dynamics in the Madison Symmetric Torus reversed-field pinch, *Phys. Plasmas* 13 (2006) 012510.
- [13] M.B. McGarry, Probing the Relationship Between Magnetic and Temperature Structures with Soft X-rays on the Madison Symmetric Torus, PhDT, 2013.
- [14] Y. Nagayama, Tomography of $m = 1$ mode structure in tokamak plasma using least-square-fitting method and Fourier-Bessel expansions, *J. Appl. Phys.* 62 (1987) 2702–2706.
- [15] M. Anton, H. Weisen, M. Dutch, W. Von der Linden, F. Buhlmann, R. Chavan, B. Marletaz, P. Marmillod, P. Paris, X-ray tomography on the TCV tokamak, *Plasma Phys. Control. Fusion* 38 (1996) 1849.
- [16] A.M. Cormack, Representation of a function by its line integrals, with some radiological applications, *J. Appl. Phys.* 34 (1963) 2722–2727.
- [17] P. Franz, F. Bonomo, G. Gadani, L. Marrelli, P. Martin, P. Piovesan, G. Spizzo, B. Chapman, M. Reyfman, High resolution soft X-ray tomography in the Madison Symmetric Torus, *Rev. Sci. Instrum.* 75 (2004) 4013–4016.